Expanding Underground. Knowledge and Passion to Make a Positive Impact on the World – Anagnostou, Benardos & Marinos (Eds)

Class A predictions of damage level in an historical fortress induced by twin tunnelling

D. Boldini & C. Spaggiari
Sapienza University of Rome, Rome, Italy

J.K. Abul
WSP-Golder, London, UK

S. Fuoco
Infrarail, Florence, Italy

E. Lusini
University of Bologna, Bologna, Italy

ABSTRACT: Tunnelling below historical city centres requires the accurate analysis of the impact of construction works on cultural heritage monuments, which need to be preserved from any possible damage. In this paper, the undercrossing of an historical masonry structure in the city of Florence (Italy), the *Fortezza da Basso*, by two tunnels of the new high-speed railway underground line is analysed. The interaction problem is studied by a 3D class-A finite element numerical model. Advanced constitutive laws are adopted to describe the key features of the mechanical behaviour of both soil layers and masonry structures. The results of the analyses show that the excavation process is likely to induce a negligible to slight damage in the historical fortress when a typical surface volume loss of 0.5% is considered in greenfield conditions.

1 INTRODUCTION

The demand for an efficient and sustainable transport has given a new impetus to the construction of underground railways in historical city centres in order to relieve pressure on existing surface lines and stations.

The case study here analysed refers to the undercrossing of *Fortezza da Basso*, a notable renaissance masonry fortress, by the twin tunnels of the new high-speed underground railway in Florence (Italy). The displacement field and the associated level of damage induced by the excavation works in the structure are predicted with a class A three-dimensional finite element model.

Firstly, the project of the new underground lines, whose construction is expected to start in 2023, is described, together with the geological and geotechnical site conditions. The interaction problem is numerically studied with a FE model developed with the commercial code Plaxis 3D®.

The Hardening Soil Model with Small Strain Stiffness (Benz 2007), calibrated against experimental static and dynamic *in situ* tests, is adopted to describe the mechanical behaviour of the soil. The Jointed Masonry Model, an equivalent elastic perfectly-plastic constitutive law, recently developed by Lasciarrea et al. (2019) modifying the Plaxis-native Jointed Rock Model, is used to seize the anisotropic plasticity of masonry. The excavation sequence of the EPB-TBM that will be adopted is simulated with a step-by-step procedure (Fargnoli et al., 2015) consisting in 86 subsequent advancements. The numerical model is validated in greenfield conditions for a 0.5% expected volume loss at the ground surface level. The simulation consists in the modelling the twin tunnel undercrossing one of the bastions of the fortress (i.e.

DOI: 10.1201/9781003348030-215

the *Cavaniglia* bastion) with a focus on the structural elements more prone to possible damage (i.e. bastion walls transversal to the tunnels). Finally, results are summarised in terms of total displacements at the soil-masonry interface and tensile strains occurring in the structure. These last are compared to threshold values, accordingly to the classification proposed by Son & Cording (2005), in order to assess the expected level of damage.

2 CASE STUDY: NEW HIGH-SPEED RAILWAY UNDERGROUND LINE

The twin tunnels of the new underground high-speed railway will be running for about 7-8 km under the *Historic Centre of Florence* (UNESCO world heritage site) with an average slope of 1.8%. The new infrastructure will link two operating lines: the Rome-Florence *Direttissima* and the Florence-Bologna HS/HC. The project also includes the construction of a new HS/HC underground train station, i.e. the Belfiore Station.

Few historical monuments will be undercrossed along the route, including *Fortezza da Basso* (Figure 1a). It is a masonry fortress with an irregular pentagon plan and five bastions located in correspondence of each corner. Only the possible effects induced on the *Cavaniglia* bastion are analysed herein (Figure 1b).

The TBM-EPB employed will be characterised by an external diameter of 9.4 m and an inner one of 8.3 m, thus allowing the transit of a type-C loading gauge. Prefabricated concrete segments 1.5 m long and 0.4 m thick will be used for the tunnel lining.

The two tunnels will not be bored simultaneously, with the even track (#S) excavated before the odd one (#N), and will run parallel at a constant distance of 19.3 m along the entire route, except for the entrance areas.

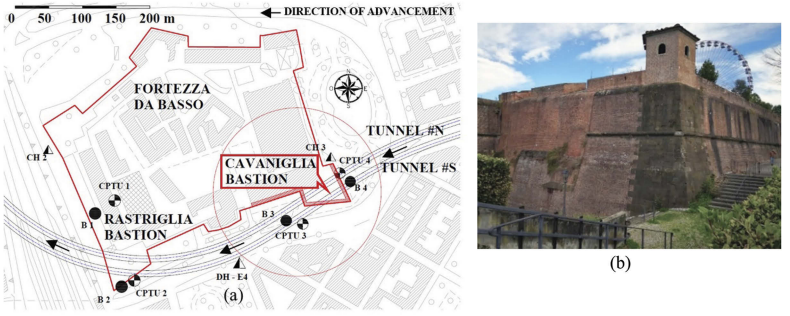

Figure 1. a) Plan view of the *Fortezza da Basso*, the two tunnels and *in-situ* investigations (B: borehole, CH: cross-hole, CPTU: cone penetration tests with piezocone); b) *Cavaniglia* bastion (from Abul 2021).

3 GEOTECHNICAL AND STRUCTURAL MODELS

The tunnel excavation will mainly interest the quaternary lacustrine and alluvial deposits of the Florence-Prato-Pistoia basin, the Arno River, and its main tributaries (Passante AV Executive Design 2021).

The geotechnical characterization of the *Fortezza da Basso* area is carried out considering the results of the laboratory and site tests conducted during the 1997, 1998 and 2007 campaigns. Site investigations (Figure 1a) included four boreholes, three in-hole seismic tests (CH and DH), and four cone penetration tests with piezocone (CPTU). Laboratory tests consisted of particle size distribution analysis, Atterberg limits test and oedometric and triaxial compression tests.

A 4-layer geotechnical model, also considering the available literature data (Vannucchi et al. 2003), is defined in Table 1. The last layer SL3 was investigated only through cross-hole and down-hole seismic tests. The water table is located at 9.5 m below the ground surface (+39.25 m a.s.l.) and hydraulic conditions can be assumed as hydrostatic. Mechanical,

physical and state parameters are summarised in Table 2. K_0 values are derived from the equations of Jaky (1944) and Mayne & Kulhawy (1982) respectively for coarse-grained and over-consolidated fine-grained strata.

Fortezza da Basso was built during the first half of the 16th century by the will of the House of Medici. The geometry of bricks and the thickness of the mortar joints is based on the "Florentine arm" (i.e. unit of length equal to 58.36 cm). Bricks are approximately 30-cm long (1/2 of the unit), 15-cm wide (1/4 of the unit), and 6-cm thick (1/8 of the unit). The mechanical properties are selected consistently with experimental tests on masonry specimens (Binda et al. 1994), since specific tests for this monument are not available (Figure 2, Table 3).

Table 1. Site stratigraphy.

Layer	Elevation (m a.s.l.) from	to	Description
R	+48.75	+41.90	made ground: coarse-grained material in a silty-clayey matrix
SA8/SF3	+41.90	+22.55	gravelly-sandy layer in silty matrix
SL5	+22.55	+13.75	silty-clayey layer
SL3	+13.75	-5.00	gravelly-sandy layer in a silty matrix

Table 2. Physical, state and mechanical properties of the soil layers.

Layer	I_p (%)	I_c	e_0	Dr (%)	φ' (°)	OCR	K_0 (-)	c_u (kPa)
R	-	-	-	58	41.5	-	0.3374	-
SA8/SF3	-	-	-	63	39	-	0.3707	-
SL5	20	1.24	0.61	-	25	2.5	0.8504	182
SL3	-	-	-	-	-	-	0.4122	-

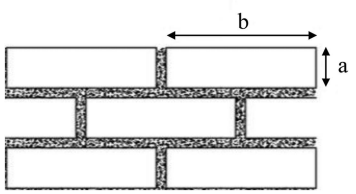

Figure 2. Definition of the brick dimensions (after Lasciarrea et al. 2019).

Table 3. Assumed properties of the masonry.

Parameters	Masonry
E (MPa)	1300
ν (-)	0.18
γ (kN/m^3)	18
a (mm)	60
b (mm)	291.8

4 NUMERICAL MODEL

Figure 3 shows the developed 3D numerical model, whose domain size is 180 m in width, 53.75 m in height and 200 m in length (Abul 2021), sufficiently large to minimize boundary effects in the internal zone of interest. The nodes at the base of the model (z = -53.75 m) are completely constrained, while horizontal movements are prevented on the side boundaries. Both the subsoil and the structure are modelled with 10-node tetrahedral elements. Dimensionless interface elements are modelled under the bastion foundations and along the perimetral walls in contact with the soil (Figure 3b) in order to better describe the real discontinuity between the soil and the structure. The interface elements connect the nodes of the soil to the nodes of the structure through reduced elastic and strength properties, thus allowing the linked meshes to follow different deformations. The interface tensile and shear strength parameters are derived from those of the surrounding soil parameters through a reduction

factor R_{inter} = 2/3, while interface elastic parameters, G_i and ν_i. are defined according to Equations 1 and 2, respectively (PLAXIS 2021).

$$G_i = R_{inter}^2 G_{soil} \tag{1}$$

$$\nu_i = 0.45 \tag{2}$$

The numerical analysis is performed in terms of effective stresses, assuming drained conditions for the coarse-grained layers and undrained ones for fine-grained layers, in accordance with *in-situ* permeability measures.

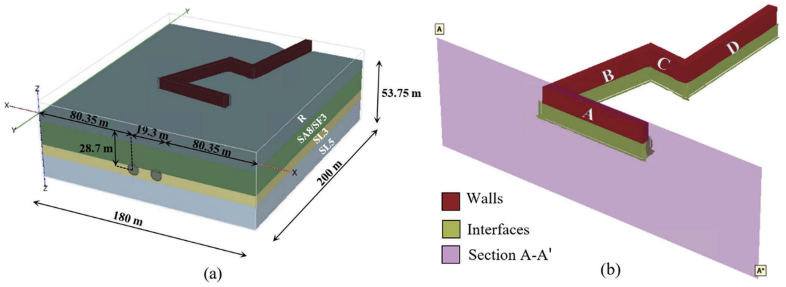

Figure 3. 3D model: (a) computational domain; (b) *Cavaniglia* bastion with interface elements below the ground level and the section (A-A') used to plot the main results (after Abul 2021).

4.1 *Excavation sequence*

For each tunnel, the excavation process is simulated for 169.5 m, the first 30.0 m of which in a single phase in order to reduce the overall computational cost. The remaining 139.5 m, that directly interact with the bastion, are divided into 93 portions, each corresponding to an advancement of the excavation face of a length equal to the lining segment (1.5 m).

Each TBM advancement is simulated by moving forward the shield for a length of 1.5 meters and deactivating the corresponding soil cluster, while dry conditions are imposed at the new boundary (internal walls and face of the tunnel segment). A face-support pressure equal to the total horizontal lithostatic stress is applied to the new excavation face, varying linearly from 353 kPa at the crown to 588 kPa at the invert. The TBM shield has a total length of 10.5 m (subdivided into 7 elements of 1.5 m each) and a thickness of 0.17 m, and it is modelled by means of steel plate elements. To control the subsidence volume, a linearly variable contraction is applied along the shield to simulate its truncated cone geometry. In particular, a linearly variable contraction is employed for elements from no. 1 to 6, with the aim of achieving the target V_L at the ground surface, while a uniform contraction is applied to the shield tail (element no. 7).

A mortar injection pressure is considered between the shield tail and the lining over a portion of soil equal to 1.5 m, while a distributed load corresponding to the hydraulic jacks thrust is applied longitudinally against the final lining. The grouting pressure is variable with depth (383 kPa at the crown and 618 kPa at the invert), with a linear increase of 25 kPa/m, while the thrust of the hydraulic jacks is set equal to 7135 kPa (Passante AV Executive Design 2021). The lining activation is simulated at 12 m distance from the excavation face, where the installation of the class C40/50 concrete ring segments is simulated through the activation of plate elements.

The schematization of the excavation steps is shown in Figure 4. Table 4 lists the properties of the shield and lining segments, which are assumed as linear elastic and isotropic.

4.2 *Constitutive models: Hssmall and JMM*

The constitutive models for the soil layers and the masonry structure are the Hardening Soil Model with Small Strain Stiffness (Hssmall) and the Jointed Masonry Model (JMM), respectively.

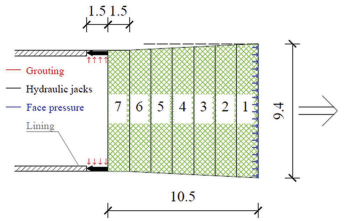

Figure 4. Schematization of the excavation steps of TBM-EPB (after Fargnoli et al. 2015).

Table 4. TBM-EPB shield and lining parameters.

Parameters	Shield (steel)	Lining (concrete)
Thickness (m)	0.17	0.4
γ (kN/m^3)	247	27
ν (-)	0	0.1
E (GPa)	200	35

Hssmall (Benz 2007) is an isotropic hardening elasto-plastic model with a non-linear elastic law able to describe the dependency of soil stiffness on the stress level at very low strain, its progressive stiffness decay and early accumulation of plastic deformations.

The profile of small strain stiffness with depth is obtained by calibrating the parameters (exponent m and reference small strain shear modulus G_0^{ref}) against the cross-hole experimental results (Figure 5). Soil unit weight, overconsolidation factor, strength and stiffness parameters for Hssmall used for different layers are summarised in Table 5.

JMM (Lasciarrea et al. 2019) is an anisotropic elastic-perfectly plastic constitutive law that captures the strength anisotropy of masonry. Shear and tensile behaviour of horizontal bed joints is described through a Mohr-Coulomb criterion with a tensile cut-off. The head joints, which are characterised by an "interlocking" between bricks due to the masonry bond, present enhanced tensile and shear resistances, depending on the ratio between brick height and length. In the JMM the elastic properties of masonry derive from a homogenization procedure and are function of the elastic properties of the bricks, their geometry, and thickness of mortar joints. The Young modulus and Poisson coefficient for masonry are assumed equal to 1300 MPa and 0.18, respectively. Shear strength angle along mortar joints, f_m, and dilatancy angle, ψ, are assumed as 22°, no cohesion is considered (Table 3).

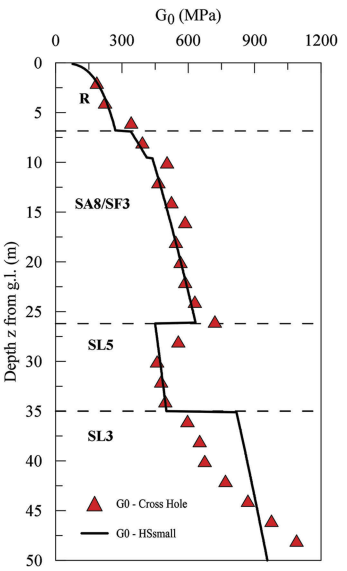

Figure 5. Calibration of HSsmall model based on results from CH test (modified after Abul 2021).

Table 5. Soil parameters for HSsmall.

Parameters	Lithotype			
	R	SA8/SF3	SL5	SL3
γ_{dry} (kN/m^3)	18.5	18.5	19.35	19.30
γ_{sat} (kN/m^3)	18.5	19.3	19.35	19.3
OCR	1	1	1	1
c' (kPa)	0	0	3.66	0
φ' (°)	41.5	39	25	36
ψ' (°)	0	0	0	0
m (-)	0.3	0.6	0.5	0.55
ν_{ur} (-)	0.2	0.2	0.25	0.2
G_0^{ref} (MPa)	350	550	270	600
E'^{ref}_0 (MPa)	840	1320	675	1440
E'^{ref}_{ur} (MPa)	168	264	202.5	288
E'^{ref}_{50} (MPa)	56	88	67.5	96
E'^{ref}_{oed} (MPa)	56	88	67.5	96
$\gamma_{0.7}$ (-)	0.0001	0.0001	0.0001	0.0001
p^{ref} (kPa)	100	100	100	100
K_0 (-)	0.3374	0.3707	0.8504	0.4122
K_0^{NC} (-)	0.3374	0.3707	0.5774	0.4122
R_f (-)	0.9	0.9	0.9	0.9

4.3 *Model validation in free-field conditions*

The validation of the model in free-field conditions is carried out on a reduced domain (85m x 132m x 53.75m) for computational reasons and limited to the excavation of a single tunnel. The aim of the analysis is to reproduce a volume loss at ground level, V_L, equal to 0.5%, considered as representative of an optimal excavation practice. The corresponding shield contraction, determined by a trial-and-error procedure, is equal to 0.7%. A comparison between the Gauss analytical curve (for V_L = 0.5% and k = 0.5) and the numerical results with HSsmall and a shield contraction of 0.7% is shown in Figure 6. The maximum subsidence in the two cases is 9.67 and 9.62 mm, respectively. Figures 6 also represents the analytical and numerical comparison in terms of longitudinal settlement curve.

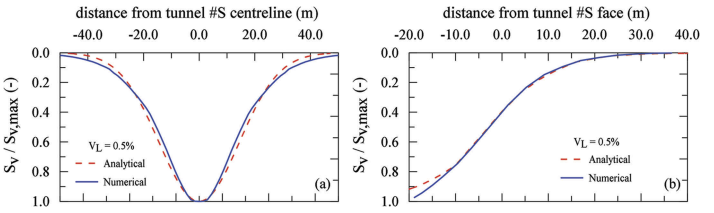

Figure 6. Normalized transversal (a) and longitudinal (b) settlement curves: comparison between the analytical curve for k=0.5 and numerical results obtained from Plaxis 3D with HSmall (modified after Abul 2021).

5 DAMAGE ESTIMATION

Results of the soil-structure interaction are presented only for wall A, which runs transversal to the railway (Figure 3b). Vertical settlements and horizontal displacements induced by tunnel excavation are shown at two different stages: after the passage of the first tunnel under the transversal wall (Figure 7); in the final conditions, after the undercrossing of both tunnels (Figure 8).

The displacement curves are plotted together with greenfield conditions for comparison and refers to the foundation depth (i.e. 8.85 m below g.l.), along a midsection running parallel to the wall (Figure 3b).

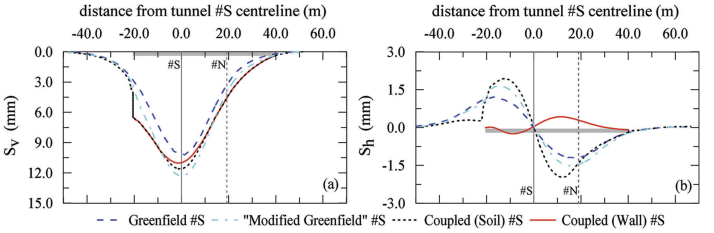

Figure 7. Comparison between numerical greenfield and coupled analyses after #S tunnel excavation: settlement curve (a) and horizontal displacement curve (b).

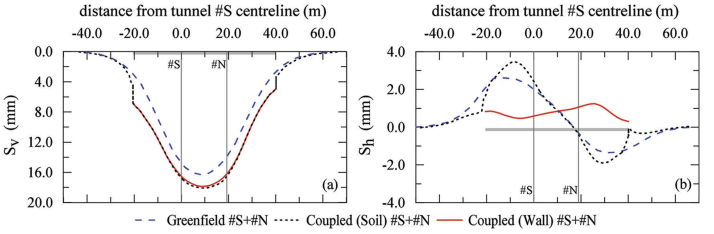

Figure 8. Comparison between numerical greenfield and coupled analyses after #N tunnel excavation: settlement curve (a) and horizontal displacement curve (b).

The presence of the structure, with its own stiffness, modifies the transversal settlement profile with respect to the greenfield conditions, producing a smaller curvature and, thus, a reduction in vertical deformation at the base of the structure (Figure 7a). On the other hand, an increase in the maximum vertical displacement is observed (i.e. +11.60 mm). This last result might be explained considering the relevant contribution given by the building own weight, which is disregarded in the greenfield analysis. In order to demonstrate the self-weight contribution, an ancillary analysis is performed, deactivating the structure and substituting its submerged part with a soil volume whose density is conveniently increased in order to match the total weight of the building. This "modified greenfield" condition is also represented in Figure 7.

In final conditions, given the small distance between the two tunnels, maximum settlements are larger than those obtained for a single tunnel (i.e. $\Delta S_{v,max}$= +6.47 mm), indicating a certain level of interaction between the two tunnels (Figure 8a).

Also, horizontal displacements in the soil are increased by the presence of the wall, when compared to greenfield condition, but they are not directly transferred to the structure thanks to the presence of interface elements around the buried portion of the wall (Figure 7b). In fact, a gap initially develops between the soil and the structure in the central part of the wall, progressively reducing its opening while distributing to a larger portion of the interface with the advancement of excavation works (Figures 7a, 8a).

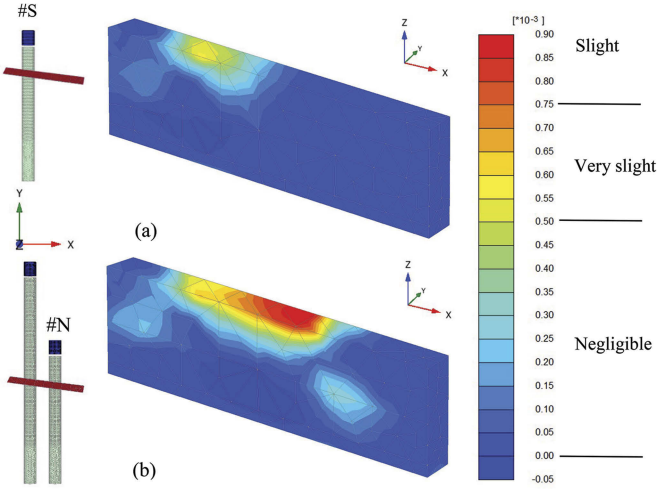

Figure 9. Tensile strain distribution in wall A after a) #S and b) #S+#N tunnel excavations.

Given the non-symmetric position of the #S tunnel with respect to the structure, the first settlements to develop are mainly concentrated on the left portion of the structure, resulting in a higher level of induced stresses and strains (Figure 9). The tensile strain plot coherently describes this phenomenon: the largest strain levels are located in the upper part of the wall, in vertical correspondence with the central axis of the first tunnel, for a maximum value of 0.065%, corresponding to a 'very slight' damage level, according to the limiting tensile strain method modified by Son & Cording (2005). Furthermore, wall A is subjected to a tie-rod mechanism, generating in the structure purely shear stresses at mid height of the wall.

The excavation of the second tunnel produces a further increase in the displacements and consequently in the strain levels of the bastion. Concerning wall A, the maximum settlements are concentrated in the central portion of the wall (Figure 8a): in fact, #N tunnel is almost symmetric to #S tunnel. Tensile strains increase in the middle-top part of the wall, as #N tunnel passage causes an enlargement of the area affected by the construction. Therefore, the maximum tensile strain increases, from a maximum value of 0.065% after the first tunnel excavation, to a maximum value of 0.089%, after the second one (Figure 9). This strain level corresponds to a 'slight' damage

category for the aforementioned classification system, which indicates negligible effects on the structure. In fact, in terms of order of magnitude, these tensile strains are perfectly in line with the strain levels associated with environmental factors affecting masonry walls during their life cycle.

6 CONCLUSION

The undercrossing of the *Fortezza da Basso* by twin tunnels is investigated through 3D coupled structural and geotechnical numerical analyses (FEM) by adopting non-linear elasto-plastic models for the soil and the structure (HSSmall and Jointed Masonry Model, respectively). Tunnel excavations are modelled to recreate a surface volume loss of 0.5%, corresponding to an optimal settlement scenario for TBM-EPB tunnelling.

From the numerical results it can be observed that the stiffness and self-weight of the structure cause a variation in the settlements with respect to greenfield conditions. In particular, the presence of the structure is associated to a reduction in the curvature of the subsidence profile with respect to greenfield conditions. Conversely, the maximum vertical displacements obtained in the coupled analysis are larger than in greenfield conditions, but, as demonstrated by the "modified greenfield" analysis, this is due to the structure self-weight. In general, the excavation of the first tunnel causes a maximum tensile strain of about 0.065% at the upper-left portion of transverse wall A, while the second tunnel produces a further increase up to a value of 0.089% at the mid top of transverse wall A. According to the limiting tensile strain method and the classification proposed by Son & Cording (2005), the overall damage category of the structure is 2, corresponding to a slight intensity. The effects on the structure associated with this damage category are negligible and comparable to those exerted by common environmental factors. In addition, it should be stressed that mitigation measures by injections and compensation grouting are also planned at the site and that, as such, the numerical predictions should be considered as conservative. The activation of compensation grouting will be based on monitoring data collected on the ground surface and on the masonry walls. More specifically, levelling with total station theodolite of vertical displacements in the ground as wells as robotic total station of 3D displacements in the structure will be collected and analysed during the tunnel excavations for a continuous comparison with attention threshold values.

REFERENCES

Abul, J.K. 2021. Studio di interazione del passante AV di Firenze con la Fortezza da Basso. *MSc thesis*. University of Bologna.

Benz, T. 2007. Small-strain stiffness of soils and its numerical consequences. *PhD thesis*. Universität Stuttgart.

Binda, L., Mirabella Roberti, G., Tiraboschi, C. & Abbaneo, S. 1994. Measuring masonry material properties, in In. Abrams, D. P., and Calvi, G. M. (eds.) *Proceedings of the U.S. Italy workshop on Guidelines for Seismic Evaluation and Rehabilitation of Unreinforced masonry buildings, Buffalo, N.Y., U.S. National Center for Earthquake Engineering Research, 20 July 1994*. pp. 3–24.

Fargnoli, V., Gragnano, C.G., Boldini, D. & Amorosi, A. 2015. 3D numerical modelling of soil–structure interaction during EPB tunnelling. *Géotechnique*. 65(1): 23–37.

Jaki, J. 1944. The coefficient of earth pressure at rest. *Journal of the Society of Hungarian Architects and Engineers*. 355–358.

Lasciarrea, W.G., Amorosi, A., Boldini, D., de Felice, G. & Malena, M. 2019. Jointed masonry model: a constitutive law for 3D soil-structure interaction analysis. *Engineering Structures*. 201, 109803.

Mayne, P. V. & Kulhawy, F. H. 1982. K0–OCR relationships in soil. *Journal of the Geotechnical Engineering Division*. 6: 851–872.

Passante AV. 2021. *Progetto Esecutivo*. Specifiche tecniche macchina di scavo.

PLAXIS, 2021. PLAXIS 3D Reference Manual. Bentley Systems International Limited, Dublin.

Son, M. & Cording, E. J., 2005. Estimation of building damage due to the excavation-induced ground movements *Journal of Geotechnical Engineering*. 131: 162–177.

Vannucchi G., Severi M. & Narcisi D. 2003. Studio di fattibilità: Sistema di Micrometropolitana per Firenze. Progettare per Firenze, Fondazione promossa dall'ente cassa di risparmio di Firenze.